

Synthesis of nanostructured pirochromite magnesium chromate with egg shell membrane template

Tholkappiyan Ramachandran¹ · Fathalla Hamed¹

Received: 6 June 2016 / Accepted: 3 August 2016 / Published online: 11 August 2016
© The Author(s) 2016. This article is published with open access at Springerlink.com

Abstract In this work, we report on the use of fresh and boiled egg shell membrane as bio-templates in the co-precipitation of pirochromite. The structure evolution, microstructure and optical properties of the ESM templated MgCr_2O_4 nanomaterial were studied by X-ray diffraction, Fourier transform infrared spectroscopy, scanning electron microscopy, Energy dispersive X-ray spectroscopy, elemental mapping and UV–Vis–NIR spectrophotometry. The annealing of the untemplated and templated co-precipitated MgCr_2O_4 powders at 1000 °C for 4 h produced single phased nanostructured material with spinel cubic crystal structure. The FTIR results showed slight variations in the band positions ν_1 and ν_2 which are attributed to the change in the microstructure due to the introduction of ESM in the preparation of MgCr_2O_4 . The morphologies and average crystallite size of the annealed MgCr_2O_4 nanocrystalline powders depended on the type of the template. 3D hierarchical flake-like and mesh like structures were observed. The annealed MgCr_2O_4 nanocrystalline powders have shown excitonic absorptions in the visible range 300–500 nm due to the transitions that took place from the O-2p level to the Cr-3d level. The optical band gap energies were found to be 3.68–3.71 eV for the direct band gap and 3.30–3.37 eV for the indirect band gap. This could make these MgCr_2O_4 nanocrystalline powders possible photocatalysts in the visible range 300–500 nm.

Keywords Pirochromite · Magnesium chromate · X-ray diffraction · Vibrational · Optical

Introduction

Spinel structures with the general chemical formula AB_2O_4 , where A, and B are two metal cations that occupy either the tetrahedral or the octahedral sites have made an impact on material science and technology. Depending on site occupancy, spinels are classified into three major types: normal, inverse, and random. Pirochromite MgCr_2O_4 is classified as normal spinel with cubic crystal structure where Mg and Cr ions occupy the tetrahedral and octahedral sites; it belongs to the space group (Fd3m), with 56 atoms per unit cell (O'Neill and Dollase 1994). MgCr_2O_4 has attracted the attention of many researchers because it could be utilized in applications such as interconnection material for solid oxide fuel cells (Schoonman et al. 1991), high temperature ceramics (Kim et al. 2001), humidity sensor elements (Drazic and Trontelj 1989), catalysts-support (Andrade et al. 2006), strengthening agents (Hashimoto and Yamagushi 1995) and combustion catalysts (Finocchio et al. 1995). In addition, MgCr_2O_4 refractories are important to the steel, cement, and copper industries (Deng et al. 2008; Ghosh et al. 2007). Recently, MgCr_2O_4 is used as an efficient complete combustant in the oxidation of propane and propene (Finocchio et al. 1994). The development of a synthesis route capable of producing MgCr_2O_4 nanomaterials with controlled size and morphology is important due to their potential applications as smart and functional materials. Various methods, such as solid state reaction (Finocchio et al. 1995), sol-gel method (SG) (Andrade et al. 2006), co-precipitation (Zhang et al. 1987), solution combustion (Arai et al. 1986), co-

✉ Fathalla Hamed
fhamed@uaeu.ac.ae

¹ Department of Physics, College of Science, United Arab Emirates University, Al Ain-15551, Abu Dhabi, United Arab Emirates

precipitation within reverse micro-emulsion (Rida et al. 2010), combustion method (Hosterman et al. 2013) and conventional double sintering ceramic technique (Khalaf et al. 2016) have been applied in the preparation of pirochromite based nanoparticles. Nevertheless, some of these methods are generally complicated, non-reliable, time-consuming, and expensive for large scale production. To overcome these limitations, a lot of efforts have been directed towards exploring facile, flexible, reliable and cost effective methods for the preparation of pirochromite based nanomaterials either by adding reducing agents or green synthesis. Among the possible alternative synthesis methods, co-precipitation synthesis is particularly attractive due to its low cost, it seems to produce a mixed oxide and it allows some degree of control on size, morphology, composition, homogeneity and surface area (Hashimoto and Yamagushi 1995). The reducing agents play a fundamental role in the precipitation of the mixed oxide. Here, sodium hydroxide (NaOH) was used as a reducing agent because it reacts non-violently in addition to being cheap and good complexant for metal cations.

Recently, template assisted nanomaterials have attracted an increasing interest because of their specific size and morphology (Balaz 2014; Oliveira et al. 2013). Compared with artificial templates, biological templates are inherently complex and hierarchical due to their fascinating structure which results in unique properties (Mann 2001). Moreover, they are generally inexpensive, abundant, and environmentally benign (Mann 2000). Biological template like eggshell membrane (ESM) has been used to synthesize the spinel nanomaterials with controlled size and hierarchically ordered microporous structures. It is widely studied because of its remarkable properties, which could be utilized in catalysis, adsorption of heavy metals [Au(I) and Au(III)] (Ishikawa et al. 2002), dyes (malachite green) (Chen et al. 2012) and organics (eosin B) (Ning and Tao 2011), biosensors (immobilized enzyme glucose oxidase) (Zheng et al. 2011), sulfonates (Wang et al. 2010) and fluorides (Lunge et al. 2012). In addition, EMS has been also used in medical industries as a possible new effective and safe therapeutic option for the treatment of pain and inflexibility associated with joint and connective tissue (JCT) disorders (Ruff et al. 2009). ESM has found applications in ophthalmology as a cheap and versatile eye model which could be used during vitreous surgery training (Benson et al. 2012). Moreover; ESM was found to represent an interesting biomaterial for electrochemical application such as a separator in supercapacitors (Li et al. 2012).

We report herein on a novel biotemplate method using ESM, environmentally friendly and natural biomembrane for preparing pirochromite MgCr_2O_4 nanostructured materials. ESM is constituted of three layers in the egg

shell (ES): (1) outer layer, (2) inner layer and (3) limiting membrane layer. The inner ESM and limiting membrane layer can be easily peeled; however, the outer ESM is strongly bonded into the calcite (CaCO_3) which is the major component in ES. To separate the outer ESM layer from the ES, a general acidic treatment has been used by various researchers such as (1) dissolving the ES in acid medium (e.g., dilute acetic acid, HCl), (2) immersing the ES in acid medium which does not completely dissolve the ES, but it will allow the separation of the ESM, (3) dissolved air flotation separation unit and (4) simply stripping the outer ESM from the ES. To the best of our knowledge, using ESM in the preparation of spinel type MgCr_2O_4 by co-precipitation is not available yet. In this research article, we report a novel biomorphic technique to obtain self-supported MgCr_2O_4 fibrous networks of nanocrystallites with high surface area using egg shell membrane (ESM) as templates. Co-precipitated templated MgCr_2O_4 on boiled or fresh ESM were prepared. The structural, morphological and optical properties of the ESM templated MgCr_2O_4 samples were characterized by X-ray diffractometry (XRD), Fourier transfer infrared spectroscopy (FTIR), Scanning electron microscopy (SEM), Energy dispersive X-ray spectrometry (EDS), and UV–Vis–NIR spectrophotometry.

Experimental

Materials

Reagent grades of chemicals were used from all chemical sources; such as magnesium nitrate hexahydrate ($\text{MgN}_2\text{O}_6 \cdot 6\text{H}_2\text{O}$, $\geq 98\%$ purity, Sigma-Aldrich), chromium (III) nitrate nonahydrate ($\text{CrN}_3\text{O}_9 \cdot 9\text{H}_2\text{O}$, 99 % purity, Sigma-Aldrich). Sodium hydroxide pellets purify LR (NaOH, 97 % purity, SDFCL fine chem limited).

Characterizations

The X-ray diffraction patterns were recorded by SHIMADZU Lab X-XRD-6100 with $\text{CuK}\alpha$ ($\lambda = 1.5418 \text{ \AA}$) line at scanning rate of $0.02^\circ/\text{min}$. FTIR measurements were performed in VARIAN 3100 FTIR, Excalibur series spectrophotometer. Small amounts of the powders were mixed with potassium bromide (KBr) and pressed into 1 mm thick discs. FTIR spectra were collected from these discs over the range $400\text{--}2300 \text{ cm}^{-1}$ at room temperature. SEM studies were performed in JEOL JSM-6010LA operated at 20 keV accelerating voltage. SEM images were obtained in the secondary electron imaging (SEI) mode. Elemental composition and mapping were obtained from the analyses of EDS. The optical absorption spectra were measured by Jasco V-670 spectrophotometer over a UV–

Vis–NIR region in the diffuse reflectance mode. Small amounts ~ 1 mg of sample powders were completely dissolved into 5 ml of ethanol to form transparent solutions. UV–Vis–NIR spectra were collected from these solutions. The light sources used are a deuterium (D2) lamp for the UV region and a halogen (WI) lamp for the VIS/NIR region.

Co-precipitation of MgCr_2O_4 nanocrystalline powders

Magnesium chromate nanocrystalline powders with the chemical formula of MgCr_2O_4 were prepared by co-precipitation technique. The starting metal nitrates were weighted in accordance with the desired nominal stoichiometric ratio and dissolved into 20 ml of de-ionized water. To get complete mixing of the solvents, the solution was stirred for 30 minutes using magnetic stirrer. Then, few grams of sodium hydroxide (NaOH) were added dropwise into the metal nitrates solution. The aqueous solution was maintained at a pH level = 12 while stirring for 4 hours at a temperature of 60 °C. Then the mixed solution was aged for 5 hours at room temperature. The aged solution was placed in the ultrasonic water bath (XUB5 series–Grant scientific instruments LTD, UK). Then, the solution was sonicated for 1.5 hours at a power of 5 W/cm². The obtained precipitates were washed with de-ionized water and acetone several times, dried in

vacuum at 100 °C for 8 hours to remove the water content. The resulted dried powder was ground using an agate mortar and pestle to a fine powder. The obtained fine powder was subjected to heat treatment at 1000 °C for 4 hours in ambient atmosphere. All experiments were carried out in ambient conditions under atmosphere. The schematic diagram represents the synthesized magnesium chromate nanocrystalline powders are shown in Fig. 1.

Separation of fresh egg-shell membrane from egg-shell

Fresh eggs were purchased from a local super market. They were gently washed with tap water to remove any albumen from the egg shell membrane, and then rinsed with de-ionized water. The eggs were carefully broken at the blunt end, yolk and white contents were manually removed. Then, the eggshells were repeatedly washed with de-ionized water. Using tweezers, the inner shell membrane and the limiting membrane were removed carefully and dipped in 10 ml hydrochloric acid to dissolve any CaCO_3 from the shell membrane. The obtained EMS was then washed in de-ionized water for three times and kept in an oven at 60 °C to remove any water content. The resulting dried membranes were used as the template for the synthesis of magnesium chromate materials. Figure 1 shows an SEM image of an egg-shell membrane. It shows the unique intricate microstructures with porous morphologies.

Fig. 1 Schematic diagram of co-precipitation of boiled egg-shell membrane templated and fresh egg-shell membrane templated of MgCr_2O_4 nanocrystalline powders

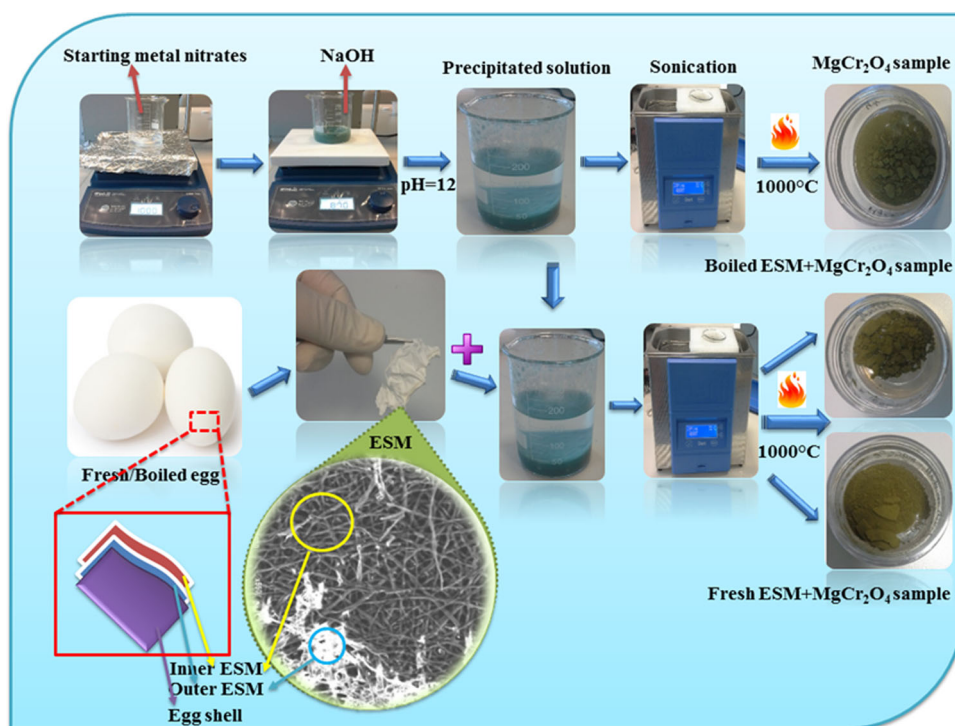
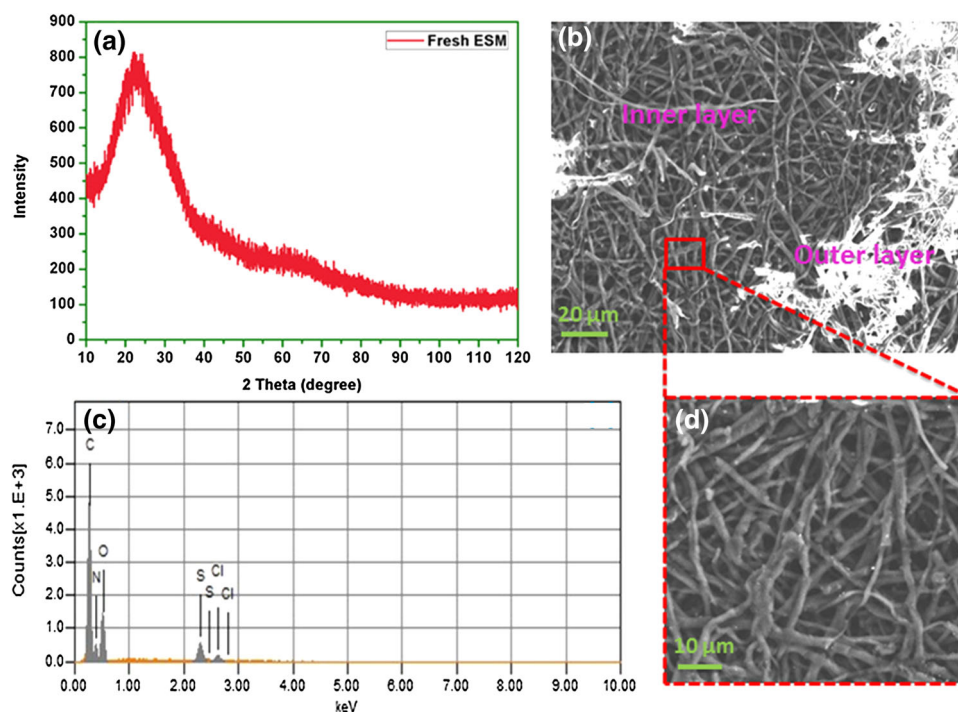


Fig. 2 **a** XRD pattern of fresh ESM, **b** SEM images of fresh ESM sample: the *inner layer* is on *left* and the *outer layer* is on *right*, **c** EDS spectra for fresh ESM, **d** magnified image of the *inner layer* of ESM



Fabrication of egg-shell membrane templated MgCr_2O_4 nanocrystalline powder

In a typical process, the egg-shell membranes were dispersed in 25 ml de-ionized water and subsequently mixed with 40 ml of co-precipitated precursor solution (“Co-precipitation of MgCr_2O_4 nanocrystalline powders”) under vigorous magnetic stirring for 4 hours. To obtain a homogeneous solution, the mixed solution was then sonicated for 1.5 hours at room temperature. The resulted product was washed with de-ionized water and acetone six times. It was then dried in vacuum at 100 °C for 8 hours to remove any water content. The resultant dried product was ground by hand with a pestle in an agate mortar to a fine powder. The obtained fine powder was subjected to heat treatment at 1000 °C for 4 hours in ambient atmosphere, then it was allowed to cool down to room temperature. A schematic representation of the formation of MgCr_2O_4 /egg-shell membrane composite is illustrated in Fig. 1.

Results and discussion

Fresh ESM studies

The XRD pattern of a fresh ESM sample is shown in Fig. 2a. The figure clearly shows the amorphous structure of the fresh ESM with a broad peak around 20°–30°. The morphology of this ESM was examined by SEM as shown in Fig. 2b. The fresh ESM is a double layer membrane, the

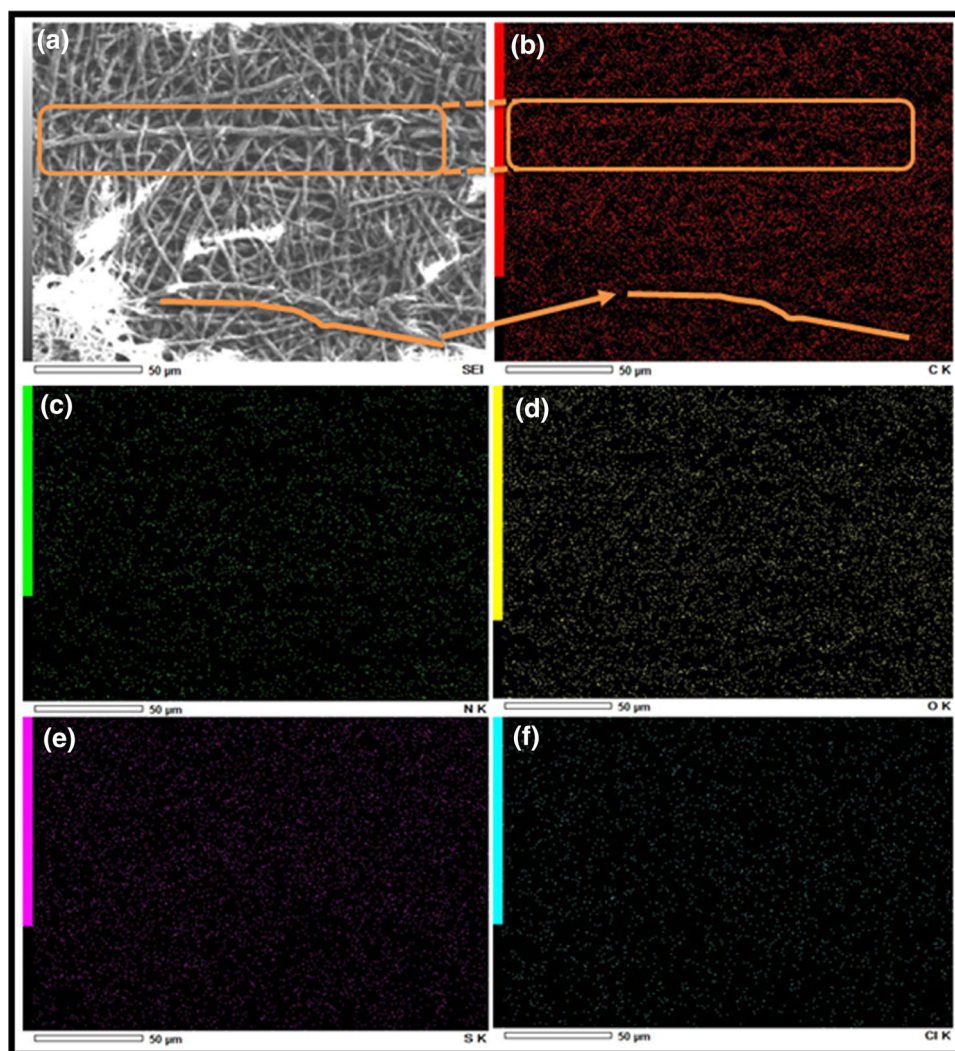
outer layer of the ESM which is on the right side of the SEM image and the inner layer of ESM which is on the left side of the SEM image. These membrane layers appeared to be porous fiber like network, composed of interlaced proteins. In comparison to the outer layer, the inner layer has spatial voids and branches in the fibrous network as shown in Fig. 2d. It appears to be more uniform with finer structure. The individual fibers have an average diameter of ~1 μm; however, they are randomly oriented.

The elemental analysis of fresh ESM was determined from EDS. Figure 2c shows the EDS spectra for the freshly prepared ESM. The analysis of these EDS spectra indicates that the presence of C, N, O, S and Cl. No other foreign elements such as Ca, Mg and P were detected in the fresh ESM. Usually these foreign elements/species are present in the calcium based egg shell. This confirms the complete removal of the egg shell membrane from the egg shell. Figure 3a–f shows the elemental mapping and distribution of C, N, O, S, and Cl within the fresh ESM sample. Different colors are subjected to the diverse emission lines where each color in the EDS mapping refers to the single emission line of C, N, O, S and Cl elements. It can be seen that the C, N, O, S, and Cl are generally well distributed and uniform. The analysis of EDS mapping indicates that these elements are incorporated within the entire fresh ESM.

Boiled ESM studies

Figure 4a shows the SEM image of the boiled ESM. It shows that the spatial voids and branches in the fibrous

Fig. 3 a SEM micrograph and b–f EDS mapping of C, N, O, S and Cl for fresh ESM sample



network had undergone shrinkage. Figure 4b shows that the fibrous network in the boiled ESM had become collapsed and coarsened into lumps that vary between 30 and 40 μm in size. Trace amount of non-volatile elements such as S and Cl were completely removed and only C, N, and O were detected in these lumps as shown in Fig. 4c.

X-ray diffraction (XRD) studies

The crystal structure of the prepared MgCr_2O_4 nanocrystalline powders was examined by X-ray diffractometer. Figure 5a shows the powder X-ray diffraction (XRD) pattern of the co-precipitated MgCr_2O_4 nanocrystalline powder annealed at 800 $^\circ\text{C}$ for 4 hours. The figure shows all the diffraction peaks (111), (220), (311), (222), (400), (331), (422), (511), (440), (531), (620), (533), (622), (441), (551), (642), (731), (800), (751), (840), and (911) that correspond to the normal spinel-cubic structure of

magnesium chromate. These peaks were well matched with JCPDS card no. 10-0351 for $Fd-3m$ space symmetric group. No additional secondary diffraction peaks were detected in the XRD pattern, which indicates the formation of single phase MgCr_2O_4 nanocrystalline powders. Figure 6a shows the XRD pattern of the as-synthesized boiled egg shell membrane templated MgCr_2O_4 sample. It shows a very broad peak near 20° – 40° , and the same thing is observed for fresh egg shell membrane templated MgCr_2O_4 sample as shown in Fig. 7a with the exception to a very weak peak near 29.3° . This peak might be due to the presence of minute traces of CaCO_3 left over from the process of dissolving the egg shell. The co-precipitated boiled and fresh ESM templated MgCr_2O_4 has shown an amorphous nature, to bring out the spinel phase of MgCr_2O_4 further calcination is needed. Similar heat treatments had to be carried out in the preparation of MgCr_2O_4 by sol-gel method (Tripathi and Nagarajan 2016).

Fig. 4 **a** SEM image, **b** magnified image and **c** EDS spectra for boiled ESM sample

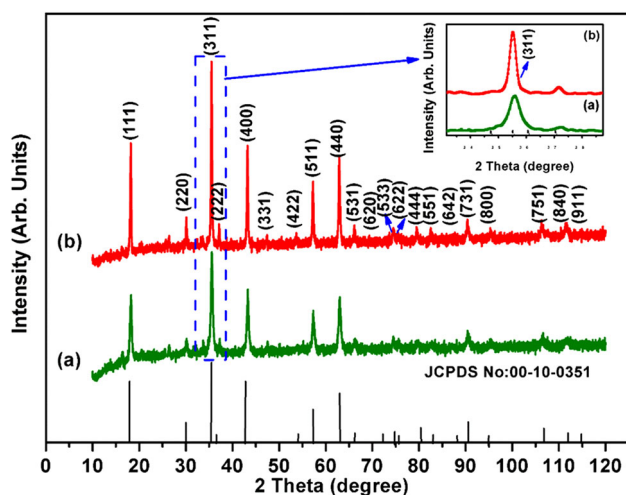
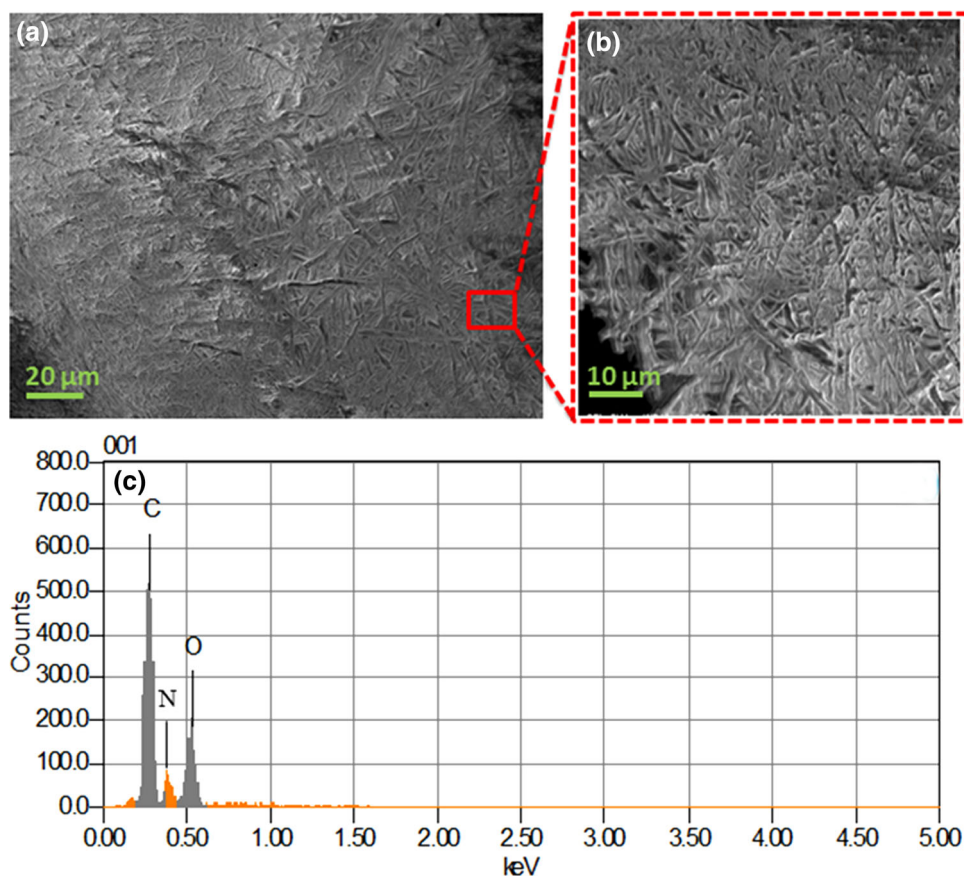


Fig. 5 X-ray diffraction (XRD) pattern of co-precipitated untemplated MgCr_2O_4 nanocrystalline powder annealed for 4 h **a** at 800 °C and **b** at 1000 °C

Heat treatments

To investigate the effect of annealing on the crystal structure of the co-precipitated MgCr_2O_4 nanocrystalline powders, samples of co-precipitated powders were annealed at 1000 °C for 4 hours. Figure 5b shows the XRD

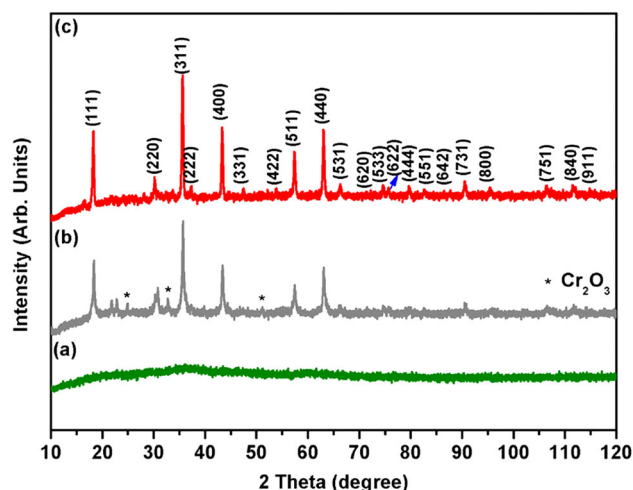


Fig. 6 X-ray diffraction (XRD) pattern of co-precipitated boiled ESM templated MgCr_2O_4 nanocrystalline powder **a** as co-precipitated, **b** annealed at 800 °C for 4 h and **c** annealed at 1000 °C for 4 h. Asterisk marks indicate peaks attributed to Cr_2O_3 phase

patterns (top curve) for the 1000 °C annealed MgCr_2O_4 sample, all the diffraction peaks match those of the 800 °C annealed sample. The peaks match very well to the crystal structure of MgCr_2O_4 in accordance with JCPDS card no. 00-010-0351. In comparison to the 800 °C annealed

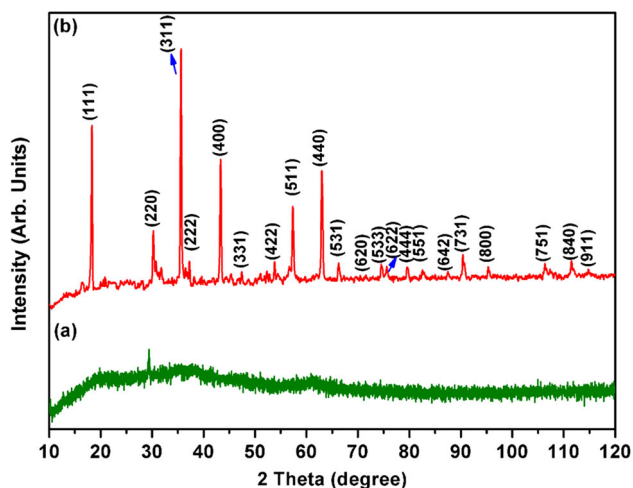


Fig. 7 X-ray diffraction (XRD) pattern of co-precipitated fresh ESM templated MgCr_2O_4 nanocrystalline powders **a** as co-precipitated and **b** annealed at 1000 °C for 4 h

MgCr_2O_4 nanocrystalline sample, the diffraction peaks of the 1000 °C annealed MgCr_2O_4 sample are more intense with less broadening as shown in the inset of Fig. 5. The higher the annealing temperature the greater the degree of crystallinity. The average crystallite size (t) of the annealed co-precipitated MgCr_2O_4 nanocrystalline powders was calculated from the Scherrer formulism in accordance with the following equation (Hamed et al. 2016),

$$t = k\lambda / (\beta \cos \theta), \quad (1)$$

where k is a constant and it is equal to 0.9, λ is the CuK_α X-ray line at 1.5405 Å, β is the full width at half maximum after instrumental broadening correction, and θ is the diffraction angle. The calculated values of average crystallite size (t) were found to be 30.8 and 63.2 nm for the 800 and 1000 °C annealed samples, respectively, these values are listed in Table 1. In comparison, these values are within range of the reported values of 28.7 nm for particles prepared by conventional solid phase reaction (Khalaf et al. 2016), 30.2 nm by sol-gel method (He 2010) and 52.4 and 6.4 nm by sol-gel and co-precipitation with reverse micro-emulsion (Rida et al. 2010).

Figure 6b and c is a presentation of the powder X-ray diffraction profiles for the annealed boiled ESM templated

MgCr_2O_4 nanocrystalline powders. The diffraction peaks of the 800 °C annealed sample do not match well with the crystal structure of MgCr_2O_4 (JCPDS card no. 00-010-0351). The additional peaks could be attributed to the presence of segregated secondary Cr_2O_3 phase. However, the diffraction peaks of the 1000 °C annealed sample match well with those of the normal spinel-cubic crystal structure of MgCr_2O_4 (JCPDS 00-010-0351). Therefore, the possible existence of a secondary (Cr_2O_3) phase in the 1000 °C annealed sample is excluded. The average crystallite size (t) of the 1000 °C annealed boiled ESM templated MgCr_2O_4 nanocrystalline powder was estimated to 46.9 nm, this is 25 % less than the 1000 °C annealed un-templated MgCr_2O_4 nanocrystalline powder. The powder X-ray diffraction pattern of the 1000 °C annealed fresh ESM templated MgCr_2O_4 nanocrystalline powder is shown in Fig. 7b. The diffraction peaks in the pattern can be indexed with the normal spinel-cubic crystal structure of MgCr_2O_4 (JCPDS no. 10-0351). The average crystallite size (t) in the 1000 °C annealed fresh ESM templated MgCr_2O_4 nanocrystalline powder was calculated to be 64.5 nm, this is approximately the same size as the one in the 1000 °C annealed un-templated MgCr_2O_4 nanocrystalline powder.

The lattice constant (a) of the 1000 °C annealed un-templated, boiled ESM templated and fresh ESM templated MgCr_2O_4 nanocrystalline powders were calculated using the following relation (Hamed et al. 2016).

$$\frac{\lambda \sqrt{h^2 + k^2 + l^2}}{2 \sin \theta} = a, \quad (2)$$

where λ is the X-ray wave length (1.5405×10^{-10} m), (hkl) are the Miller indices and θ is the diffraction angle that corresponds an (hkl) plane. The calculated values of lattice constants of the 1000 °C annealed un-templated, boiled ESM templated and fresh ESM templated MgCr_2O_4 nanocrystalline powders are 8.347, 8.323 and 8.324 Å, respectively as listed in Table 1. In comparison, these values are in good agreement with the reported values of 8.333 Å for MgCr_2O_4 (Stefanescua et al. 2011), 8.39 Å for MgFeCrO_4 (Hankare et al. 2009) and 8.381 Å for $\text{Mg}_{0.5}\text{Zn}_{0.5}\text{FeCrO}_4$ (Haralkar et al. 2012).

Table 1 Average crystallite size (t) nm, X-ray density (d_x), surface area (m^2/g), lattice constant (a) (Å) for the 1000 °C annealed co-precipitated un-templated, boiled ESM templated and fresh ESM templated MgCr_2O_4 nanocrystalline powders for 4 h

Samples annealed at 1000 °C for 4 h	Average crystallite size, t (nm)	X-ray density (d_x) g/cm^3	Surface area (S) (m^2/g)	Lattice constant (a) (Å)
Un-templated MgCr_2O_4	63.2	4.39	21.59	8.347
Boiled ESM templated MgCr_2O_4	46.9	4.42	28.84	8.323
Fresh ESM templated MgCr_2O_4	64.5	4.43	21.0	8.324

The X-ray density (d_X) of the 1000 °C annealed untemplated, boiled ESM templated and fresh ESM templated MgCr_2O_4 nanocrystalline powders were determined from the following simple relation (Hamed et al. 2016).

$$d_X = 8M/N_A V, \quad (3)$$

where M is the molecular weight of the sample, V is the unit cell volume ($V = a^3$ for cubic) and N_A is the Avogadro's number ($N_A = 6.023 \times 10^{23}/\text{mol}$). The calculated values of d_X are 4.39, 4.42 and 4.43 g/cm^3 for the un-templated, boiled ESM templated and fresh ESM templated, respectively (Table 1). These values are almost the same and are in good agreement with the reported value of 4.43 g/cm^3 for MgCr_2O_4 prepared by co-crystallization method (Haralkar et al. 2012). The specific surface area (S) of the 1000 °C annealed samples were calculated with the help of X-ray density (d_X) and average crystallite size (t) in accordance with the following expression (Hamed et al. 2016)

$$S = 6/d_X(t). \quad (4)$$

The values of specific surface area of the 1000 °C annealed un-templated, boiled ESM templated and fresh ESM templated MgCr_2O_4 nanocrystalline powders were determined to be 21.59, 28.84 and 21.0 m^2/g , respectively. The 1000 °C annealed boiled ESM templated MgCr_2O_4 nanocrystalline powder has a surface area that 33 % higher than the other two samples, this is due to its smaller average crystallite size.

Fourier transfer infrared spectroscopy (FTIR) studies

FTIR studies were conducted to shade some light on the position of the cations within the crystal structure of the 1000 °C annealed un-templated, boiled ESM templated and fresh ESM templated MgCr_2O_4 nanocrystalline powders. Figure 8 shows the recorded FTIR spectra at room temperature over the shorter wavelength range of 400–2300 cm^{-1} . The strongest observed absorption bands are within this range 400–700 cm^{-1} . These bands correspond to the intrinsic stretching vibrational bonds in the single-phase spinel structure with two sublattices: tetrahedral (A) sites and octahedral (B) sites (White and De Angelis 1967). The position and intensity of these bands depend on the nature of cations distribution and their occupancy in the sub-lattices of the spinel structure. For pirochromite, the absorption band ν_1 observed around $\sim 631 \text{ cm}^{-1}$ is attributed to the stretching vibrational mode between metal ions and oxygen ions in the tetrahedral sites; whereas the absorption band ν_2 observed around $\sim 440 \text{ cm}^{-1}$ is attributed to the stretching vibrational mode between metal ions and oxygen ions in the octahedral site. The difference between the band positions of ν_1 and ν_2 is

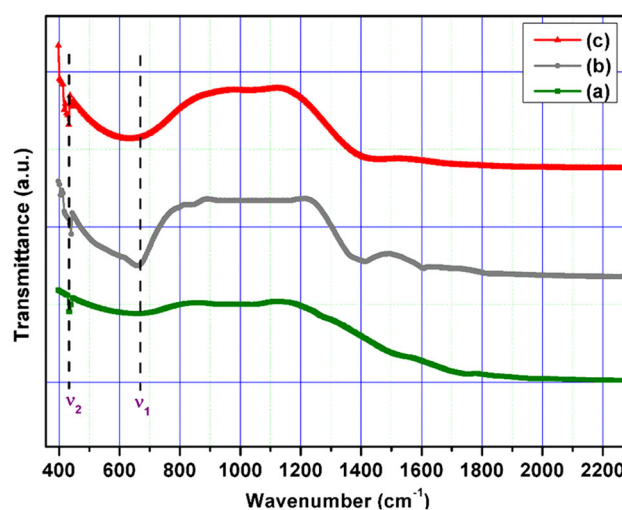


Fig. 8 FTIR spectrum of the 1000 °C annealed co-precipitated MgCr_2O_4 nanocrystalline powders for 4 h **a** un-templated, **b** boiled ESM templated and **c** fresh ESM templated

expected due to the difference in the $\text{Fe}^{3+}-\text{O}^{2-}$ bond lengths in the octahedral and the tetrahedral sites. Similar observations have been reported for various spinel systems (Morozova and Popov 2010; Bhosale and Chougule 2006; Zaki and Sc 2010). The ν_1 and ν_2 band positions in our samples are almost same, this makes us believe that we have the right cations distribution for the normal spinel-cubic structure in our MgCr_2O_4 samples.

Morphology and elemental analysis

Here we present morphological and elemental mapping and compositional studies conducted on different co-precipitated MgCr_2O_4 samples. Figure 9a, c, d, e shows SEM images of the 1000 °C annealed un-templated MgCr_2O_4 sample. The images show the formation of nano-sized structures with irregular shapes. One can find that many nanorod-like shapes (Fig. 9c, d, e) are assembled to form isolated nanoflakes. These MgCr_2O_4 nanoflakes have sharp tip ($\sim 10 \text{ nm}$), width ($\sim 190 \text{ nm}$) and lengths that range from 430 to 500 nm. The SEM image also show clusters of nanoparticles, aggregates and cube like shapes (highlighted by yellow color in Fig. 9a). The 1000 °C annealed un-templated MgCr_2O_4 sample is a mix of different nanostructured shapes. The elemental composition was determined from the analyses of energy dispersive X-ray (EDS) spectroscopy. Figure 9b is an energy dispersive spectrum of the 1000 °C annealed un-templated MgCr_2O_4 sample. The spectrum shows the presence of Mg, Cr and O. No foreign elements or impurity were detected within the limits of our EDS detector. The elemental analysis of the EDS spectrum is in good agreement with the expected nominal chemical composition of MgCr_2O_4 . The results of

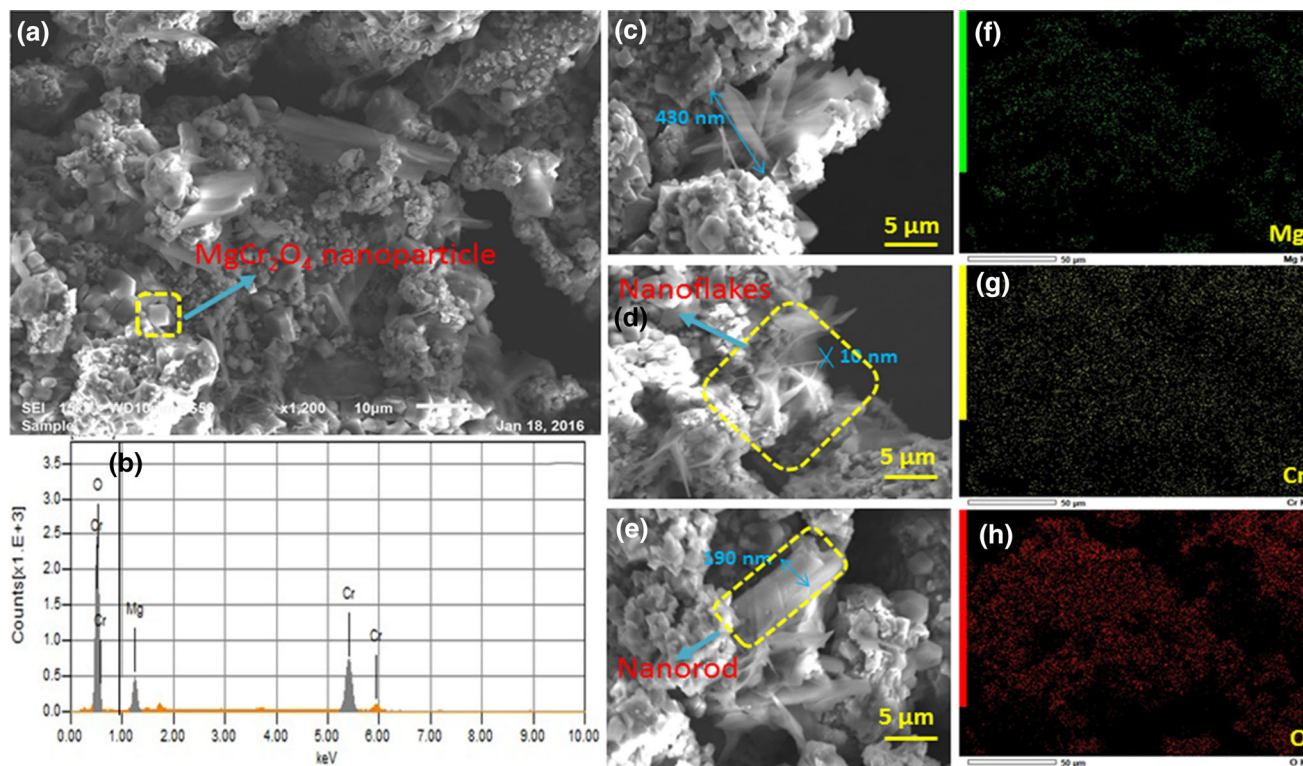


Fig. 9 **a** SEM image and **c, d, e** enlarged images of some parts in **a**, **b** EDS spectra and elemental mapping of **f** Mg, **g** Cr and **h** O for the 1000 °C annealed un-templated MgCr_2O_4 nanocrystalline powder for 4 h

the elemental mapping of the Mg, Cr and O ions within the 1000 °C annealed un-templated MgCr_2O_4 sample are presented in Fig. 9f, g, h. The results show that the constituent elements are uniformly distributed throughout the sample.

Figure 10a shows an SEM image of the 1000 °C annealed boiled ESM templated MgCr_2O_4 sample. The sample essentially shows the same features as the un-templated sample where aggregates of MgCr_2O_4 nanoparticles overlapped with flakes to form mesh like structures; however, the average crystallite size (t) is 25 % less as discussed earlier in “Fresh ESM studies”. Figure 10b is an EDS spectrum of the present sample. The analysis of the spectrum revealed the desired nominal chemical composition while the elemental mapping in Fig. 10c, d, e, f indicated uniform distribution of the constituent elements within the 1000 °C annealed boiled ESM templated MgCr_2O_4 sample. The SEM images of the 1000 °C annealed fresh ESM templated MgCr_2O_4 sample are presented in Fig. 11a, c, d, e. The images show morphologies that are quite different than the previous two cases. 3D hierarchical flake-like structure is seen with less pores. The analyses of EDS spectra presented in Fig. 11b gave a composition that correspond to the stoichiometric ratios of MgCr_2O_4 . The elemental mapping in Fig. 11f, g, h indicated a uniform distribution of the elements throughout the entire sample.

UV/Vis/NIR spectroscopy studies

The optical absorption of the 1000 °C annealed un-templated, boiled ESM templated and fresh ESM templated MgCr_2O_4 nanocrystalline powders was investigated by UV/Vis/NIR spectroscopy. Figure 12 shows the optical reflectance spectra of the three samples (un-templated, boiled ESM template, and fresh ESM templated). The spectra suggest an excitonic absorption behavior in the visible range 300–500 nm. The electronic transitions are from the valence band to the conduction band (O-2p level into the Cr-3d level). The optical absorbance coefficient (α) of the three samples were calculated from the following equation (Lajunen and Peramaki 2004),

$$\alpha d = \ln(1/T), \quad (5)$$

where d is the path length ($d = 1$ cm) and T is the transmittance. The transmittance (T) was calculated from the measured absorbance (A) using the relation (Lajunen and Peramaki 2004):

$$A = -\text{Log}_{10}(T). \quad (6)$$

The insert to Fig. 12 shows plots of the absorption coefficient (α) as a function of wavelength for three samples. It can be seen that the absorption coefficients tend to increase from 300 nm and reaches a maximum at 374 nm and then

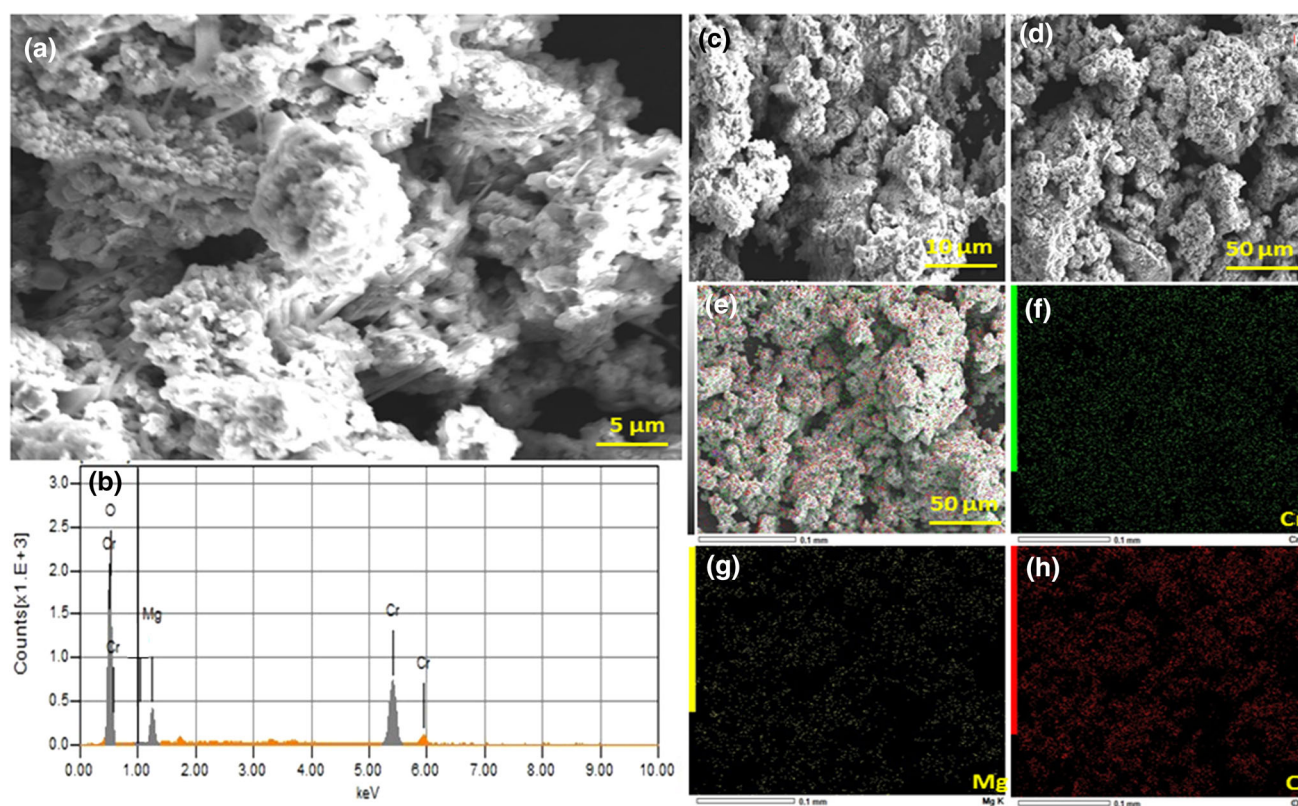


Fig. 10 **a, c, d** SEM image, **b** EDS spectra and elemental mapping of **g** Mg, **f** Cr and **h** O and **e** elemental distribution for the 1000 °C annealed boiled ESM templated MgCr_2O_4 nanocrystalline powder for 4 h

decrease as the wavelength increases. This could be attributed to inelastic scattering of charge carriers by phonons, lattice deformations and internal electric fields within the crystals. Similar behavior was observed for many semiconducting materials (Willardson and Beer 1967).

The optical band gap energies of the 1000 °C annealed un-templated, boiled ESM templated and fresh ESM templated MgCr_2O_4 nanocrystalline powders were calculated from the wavelength value corresponding to the intersection point of the vertical and horizontal part of the spectrum, in accordance with following simple relation (Hamed et al. 2016),

$$E_g = 1240/\lambda, \quad (7)$$

where E_g is the band gap energy (eV) and λ is the wavelength in (nm). The calculated values of energy band gap from the above relation correspond to the absorption limit. These values are listed in Table 2. In order to get more precise values of the optical band gaps, the values of E_g were calculated with the help of the Tauc equation (Hamed et al. 2016),

$$(\alpha E_p) = C(E_p - E_g)^m, \quad (8)$$

where E_p ($E_p = h\nu$) is the incident photon energy, C is a constant that depends on the transition probability and

m depends on the nature of the optical absorption transition (Hamed et al. 2016). The value of m is 1/2 for direct allowed electronic transition (direct band gap) and 2 for indirect allowed electronic transition (indirect band gap) (Zaki and Sc 2010). For this purpose, $(\alpha h\nu)^{1/2}$ was plotted as a function of photon energy $h\nu$ (eV) for the indirect gap and $(\alpha h\nu)^2$ against photon energy $h\nu$ (eV) for the direct gap. Figure 13 is presentation of these plots. The linear intercept at the $h\nu$ on x-axis (shown in Fig. 13) gives the value of the optical bandgap. The estimated optical band gap energies are listed in Table 2. The band gap energies for the three samples are very close, they range from 3.68 to 3.71 eV for the direct band gap and from 3.30 to 3.37 eV for the indirect band gap. These values are not too far from the reported value of 3.4 eV for normal spinel ZnCr_2O_4 (Parhia and Manivannan 2008). The 1000 °C annealed un-templated, boiled ESM templated and fresh ESM templated MgCr_2O_4 nanocrystalline powders are sensitive to visible light which could make them suitable photocatalysts (Borse et al. 2011; Parhia and Manivannan 2008).

From the preceding sections, we can say that the use of ESM as a template in the co-precipitation of MgCr_2O_4 has an effect on the morphologies and the crystallite grain sizes in the annealed templated MgCr_2O_4 nanocrystalline powders. At 1000 °C, the ESM is completely burnt out and none of it is

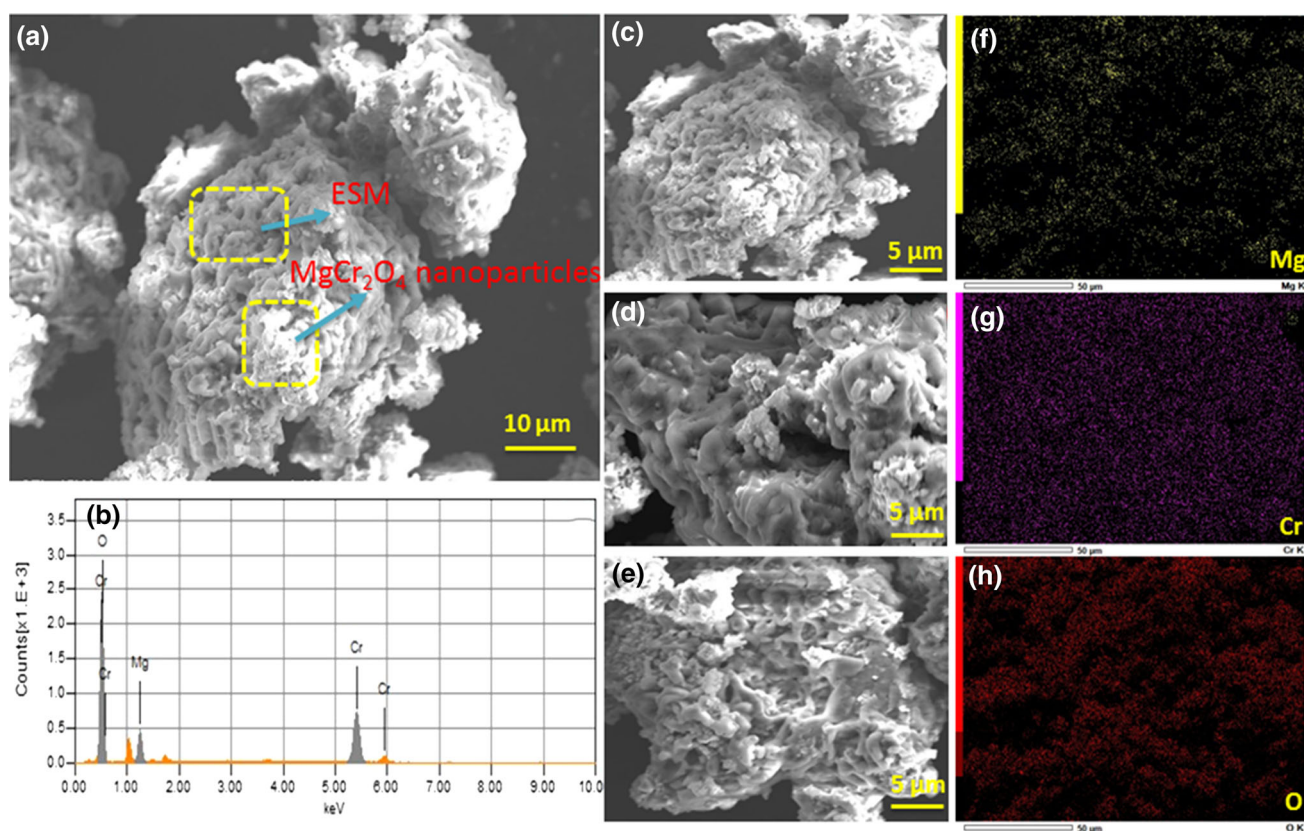


Fig. 11 a SEM image, b EDS spectra and elemental mapping of c Mg, d Cr and e O and e elemental distribution for the 1000 °C annealed fresh ESM templated MgCr₂O₄ nanocrystalline powder for 4 h

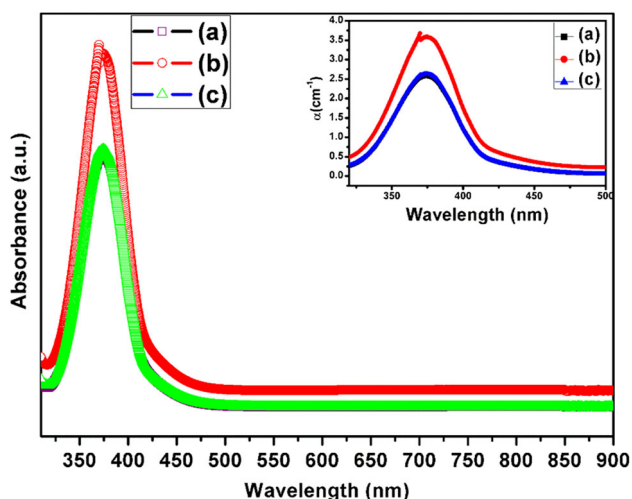


Fig. 12 UV absorbance spectra for of the 1000 °C annealed MgCr₂O₄ nanocrystalline powder for 4 h a un-templated, b boiled ESM templated and c fresh ESM templated

left within the annealed MgCr₂O₄ nanocrystalline powders. It seems that the ESM plays a role during the co-precipitation stage and possibly during the annealing stage when the temperature is raised from room temperature to 1000 °C. A simple experiment has confirmed the disappearance of ESM

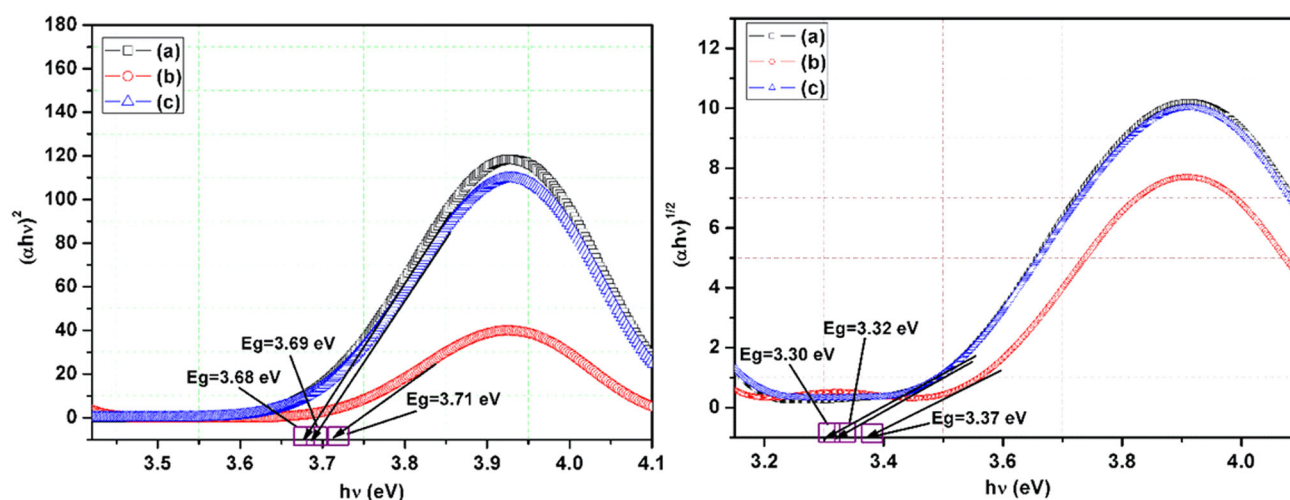
when it was annealed in a matter of 15 min. As far as we know, there are no reports on the optical band gap energies of nanocrystalline MgCr₂O₄ except for the report by Tripathi et al. They have reported a value of 1.71 eV for MgCr₂O₄ nanoparticles (Tripathi and Nagarajan 2016), we feel that this value is too low in comparison of 3.46 eV reported by Peng et al. for ZnCr₂O₄ nanoparticles (Peng and Gao 2008) even though both groups reported similar features in their optical absorption spectra. Both groups reported two extra peaks centered on 440 nm and 600 nm in their optical absorption spectra which we do not observe for our nanocrystalline MgCr₂O₄ powders. Here we have reported optical band gap energies of nanocrystalline MgCr₂O₄ powders. There were small variations in the values of the optical band gap energies between the different samples. There was also a little shading in the color of the three nanocrystalline MgCr₂O₄ powders.

Conclusion

Fresh and boiled eggshell membranes (ESM) were used as a biotemplates during the co-precipitation of pirochromite MgCr₂O₄. The un-templated and templated co-precipitated

Table 2 Optical band gap energies for the 1000 °C annealed un-templated, boiled ESM templated and fresh ESM templated MgCr_2O_4 nanocrystalline powders for 4 h

Samples annealed at 1000 °C for 4 h	Band gap (eV)		
	Simple method	Kubelka–Munk function	
		Direct	Indirect
Un-templated MgCr_2O_4	3.41	3.68	3.30
Boiled ESM templated MgCr_2O_4	3.53	3.71	3.37
Fresh ESM templated MgCr_2O_4	3.43	3.69	3.32

**Fig. 13** Tauc plots for direct band gap (left side) and indirect band gap (right side) for the 1000 °C annealed MgCr_2O_4 nanocrystalline powders for 4 h **a** un-templated, **b** boiled ESM templated and **c** fresh ESM templated

MgCr_2O_4 powders were subjected to heat treatment at 1000 °C for 4 h to produce single phase nanocrystalline MgCr_2O_4 powders with spinel cubic crystal structure. The un-templated and templated nanocrystalline MgCr_2O_4 powders were characterized by XRD, FTIR, SEM, EDS and UV/Vis/NIR spectroscopy. The morphologies and the crystallite grain sizes of the 1000 °C annealed templated nanocrystalline MgCr_2O_4 powders were found to depend on whether the ESM is boiled or fresh. The fresh ESM templated nanocrystalline MgCr_2O_4 powders were found to form 3D hierarchical cascading flake-like structure, the boiled ESM templated nanocrystalline MgCr_2O_4 formed mesh like structures whereas the un-templated nanocrystalline MgCr_2O_4 powders were found to form nano-sized structures with irregular shapes. The un-templated and templated nanocrystalline MgCr_2O_4 powders were found to be sensitive to visible light absorption over the range 300–500 nm. This could make them possible photocatalysts over this range. The optical band gap energies were found to vary from 3.68 to 3.71 eV for the direct band gap and from 3.30 to 3.37 eV for the indirect band gap. The

concept of using ESM as a template should be extended to other metal oxides nanomaterial.

Acknowledgments This research was supported by the UAEU Program for Advanced Research (UPAR) under grant G00001647, UAE University, Al Ain, United Arab Emirates.

Open Access This article is distributed under the terms of the Creative Commons Attribution 4.0 International License (<http://creativecommons.org/licenses/by/4.0/>), which permits unrestricted use, distribution, and reproduction in any medium, provided you give appropriate credit to the original author(s) and the source, provide a link to the Creative Commons license, and indicate if changes were made.

References

- Andrade MJ, Lima MD, Bonadiman R, Bergmann CP (2006a) Nanocrystalline pirochromite spinel through solution combustion synthesis. *Mater Res Bull* 41:2070–2079
- Andrade MJ, Lima MD, Bonadiman R, Bergmann CP (2006b) Nanocrystalline pirochromite spinel through solution combustion synthesis. *Mater Res Bull* 41:2070–2079

- Arai H, Yamada T, Eguchi K, Seiyama T (1986) Catalytic combustion of methane over various perovskite-type oxides. *Appl Catal* 26:265–276
- Balaz M (2014) Eggshell membrane biomaterial as a platform for applications in materials science. *Acta Biomater* 10:3827–3843
- Benson KF, Ruff KJ, Jensen GS (2012) Effects of natural eggshell membrane (NEM) on cytokine production in cultures of peripheral blood mononuclear cells: increased suppression of tumor necrosis factor- α levels after in vitro digestion. *J Med Food* 15:360–368
- Bhosale AG, Chougule BK (2006) X-ray, infrared and magnetic studies of Al-substituted Ni ferrites. *Mater Chem Phys* 97:273–276
- Borse PH, Jang JS, Lee JS, Khan FN, Ha MG, Kim JP, Bae JS, Jeong ED, Kim HG (2011) Enhanced photocatalytic properties due to electron-rich Ti-ion doping in ZnFe_2O_4 under visible light irradiation. *J Korean Phys Soc* 59:2750–2755
- Chen H, Liu J, Cheng X, Peng Y (2012) Adsorption for the removal of malachite green by using eggshell membrane in environment water samples. *Adv Mater Res* 573–754:63–67
- Deng YY, Wang HZ, Zhao HZ (2008) Influence of chrome-bearing sols vacuum impregnation on the properties of magnesia-chrome refractory. *Ceram Int* 34:573–580
- Drazic G, Trontelj M (1989) Preparation and properties of ceramic sensor elements based on MgCr_2O_4 . *Sens Actuators* 18:407–414
- Finocchio E, Busca G, Lorenzelli V, Willey RJ (1994) FTIR studies on the selective oxidation and combustion of light hydrocarbons at metal oxide surfaces. Propane and propene oxidation on MgCr_2O_4 . *J Chem Soc Faraday Trans* 90:3347–3356
- Finocchio E, Busca G, Lorenzelli V, Willey RJ (1995a) The activation of hydrocarbon C–H bonds over transition metal oxide catalysts: a FTIR study of hydrocarbon catalytic combustion over MgCr_2O_4 . *J Catal* 151:204–215
- Finocchio E, Busca G, Lorenzelli V, Willey RJ (1995b) The activation of hydrocarbon C–H bonds over transition metal oxide catalysts: a FTIR study of hydrocarbon catalytic combustion over MgCr_2O_4 . *J Catal* 151:204–215
- Ghosh A, Haldar MK, Das SK (2007) Effect of MgO and ZrO_2 additions on the properties of magnesite-chrome composite refractory. *Ceram Int* 33:821–825
- Hamed F, Tholkappian R, Vishista K (2016) The effect of induced strains on the optical band gaps in lanthanum doped zinc ferrite nanocrystalline powders. *Mod Phys Lett B* 30:1650230
- Hankare PP, Vader VT, Sankpal UB, Gavali LV, Sasikala R, Mulla IS (2009) Effect of sintering temperature and thermoelectric power studies of the system $\text{MgFe}_{2-x}\text{Cr}_x\text{O}_4$. *Solid State Sci* 11:2075–2079
- Haralkar SJ, Kadam RH, More SS, Shirsath SE, Mane ML, Patil S, Mane DR (2012) Substitutional effect of Cr^{3+} ions on the properties of Mg–Zn ferrite nano particles. *Phys B* 407:4338–4346
- Hashimoto S, Yamaguchi A (1995) Growth of MgCr_2O_4 whiskers. *J Cryst Growth* 154:329–333
- He H (2010) Catalysis and photocatalysis of MgCr_2O_4 powder at room temperature. *Recent Pat Chem Eng* 3:74–77
- Hosterman BD, Farley John W, Johnson Allen L (2013) Spectroscopic study of the vibrational modes of magnesium nickel chromite, $\text{Mg}_x\text{Ni}_{1-x}\text{Cr}_2\text{O}_4$. *J Phys Chem Solids* 74:985–990
- Ishikawa S, Suyama K, Arihara K, Itoh M (2002) Uptake and recovery of gold ions from electroplating wastes using eggshell membrane. *Bioresour Technol* 81:201–206
- Khalaf KAM, Al-Rawas AD, Widatallah HM, Al-Rashdi KS, Sellai A, Gismelseed AM, Hashim M, Jameel SK, Al-Ruqeishi MS, Al-Riyami KO, Shongwe M, Al-Rajhi AH (2016) Influence of Zn^{2+} ions on the structural and electrical properties of $\text{Mg}_{1-x}\text{Zn}_x\text{FeCrO}_4$ spinels. *J Alloys Compd* 657:733–747
- Kim BN, Hiraga K, Morita K, Sakka Y (2001) A high-strain-rate superplastic ceramic. *Nature* 413:288–291
- Lajunen LHM, Peramaki P (2004) Spectrochemical analysis by atomic absorption and emission. Royal Society of Chemistry, Cambridge
- Li Z, Zhang L, Amirkhiz BS, Tan X, Xu Z, Wang H, Olsen BC, Holt CMB, Mitlin D (2012) Carbonized chicken eggshell membranes with 3D architectures as high-performance electrode materials for supercapacitors. *Adv Energy Mater* 2:431–437
- Lunge S, Thakre D, Kamble S, Labhsetwar N, Rayalu S (2012) Alumina supported carbon composite material with exceptionally high defluorination property from eggshell waste. *J Hazard Mater* 237:161–169
- Mann S (2000) The chemistry of form. *Angew Chem Int Ed Engl* 39:3392–3406
- Mann S (2001) Biomineralization. Principles and concepts in bioinorganic materials chemistry. Oxford University Press, Oxford
- Morozova LV, Popov VP (2010) Synthesis and investigation of magnesium chromium spinel. *Glass Phys Chem* 36:86–91
- Ning L, Tao L (2011) Adsorption and decoloration of nitroso dye based on eggshell membrane. *Adv Mater Res* 183–185:963–966
- O'Neill HSC, Dollase WA (1994) Crystal structures and cation distributions in simple spinels from powder XRD structural refinements: MgCr_2O_4 , ZnCr_2O_4 , Fe_3O_4 and the temperature dependence of the cation distribution in ZnAl_2O_4 . *Phys Chem Miner* 20:541–555
- Oliveira DA, Benelli P, Amante ER (2013) A literature review on adding value to solid residues: egg shells. *J Clean Prod* 46:42–47
- Parhia P, Manivannan V (2008) Microwave metathetic approach for the synthesis and characterization of ZnCr_2O_4 . *J Eur Ceram Soc* 28:1665–1670
- Peng C, Gao L (2008) Optical and photocatalytic properties of spinel ZnCr_2O_4 nanoparticles synthesized by a hydrothermal route. *J Am Ceram Soc* 91:2388–2390
- Rida K, Benabbas A, Bouremmad F, Pena MA, Martinez-Arias A (2010) Influence of the synthesis method on structural properties and catalytic activity for oxidation of CO and C_3H_6 of pirochromite MgCr_2O_4 . *Appl Catal A* 375:101–106
- Ruff KJ, DeVore DP, Leu MD, Robinson MA (2009) Eggshell membrane: a possible new natural therapeutic for joint and connective tissue disorders. Results from two open-label human clinical studies. *Clin Interv Aging* 4:235–240
- Schoonman J, Dekker JP, Broers JW (1991) Electrochemical vapor deposition of stabilized zirconia and interconnection materials for solid oxide fuel cells. *Solid State Ion* 46:299
- Stefanescu M, Barbu M, Vlase T, Barvinschi P, Barbu-Tudoran L, Stoia M (2011) Novel low temperature synthesis method for nanocrystalline zinc and magnesium chromites. *Thermochim Acta* 526:130–136
- Tripathi VK, Nagarajan R (2016) Rapid synthesis of mesoporous, nano-sized MgCr_2O_4 and its catalytic properties. *J Am Ceram Soc* 99:814–818
- Wang WD, Chen B, Huang YM, Cao J (2010) Evaluation of eggshell membrane-based bio-adsorbent for solid-phase extraction of linear alkylbenzene sulfonates coupled with high-performance liquid chromatography. *J Chromatogr A* 1217:5659–5664
- White WB, De Angelis BA (1967) Interpretation of the vibrational spectra of spinels. *Spectrochim Acta A* 23:985–995
- Willardson RK, Beer AC (1967) Semiconductor and semimetals: optical properties of III–V compounds. Academic Press, New York

- Zaki SM, Sc M (2010) Thesis in physics, Faculty of science. Tanta University, Egypt
- Zhang HM, Teraoka Y, Yamazoe N (1987) Preparation of perovskite-type oxides with large surface area by citrate process. *Chem Lett* 16:665–668
- Zheng BZ, Xie SP, Qian L, Yuan HY, Xiao D, Choi MMF (2011) Gold nanoparticles coated eggshell membrane with immobilized glucose oxidase for fabrication of glucose biosensor. *Sens Actuators B Chem* 152:49–55